Journal of Porous Materials (2024) 31:1777–1787
https://doi.org/10.1007/s10934-024-01625-5

In situ synthesis of three-dimensional electrospun polyacrylonitrile nanofiber network reinforced silica aerogel for high-efficiency oil/water separation

Yi-Ming Li[1,2] · Fang Liu[2] · Zhen-Zhen Jia[1,2] · Xuan Cheng[1,3] · Yu-Ming Zheng[2] · Zai-Dong Shao[2]

Accepted: 27 April 2024 / Published online: 19 May 2024

Abstract
In situ electrospun 3D polyacrylonitrile (PAN) nanofiber-reinforced (EPNR) silica aerogel monoliths were prepared through methyltriethoxysilane–trimethylchlorosilane modification followed by ambient pressure drying (APD). The 3D PAN nanofiber network was built into silica sol by liquid-assisted collection. Homodispersed and intertwined PAN nanofibers were well incorporated into the silica aerogel matrix. The APD-EPNR silica aerogel had a porosity of 90.9% and a BJH pore volume of 2.15 $cm^3\ g^{-1}$. Furthermore, the APD-EPNR silica aerogel monolith showed excellent flexibility and revealed a highly hydrophobic surface with a water contact angle of 145°. The APD-EPNR aerogel was suitable for removal of oil from water. The static mass of the APD-EPNR silica aerogel achieved 700%–1500% to various solvents and the aerogel can be recovered without obvious performance decline. The APD-EPNR silica aerogel mat also achieved oil/water separation with a separation efficiency of more than 99%. Hence, the prepared APD-EPNR silica aerogel has promising application for treatment of oil pollution.

Keywords Silica aerogel · Electrospinning · Reinforce · Hydrophobic · Oil/Water separation

1 Introduction

Many industries generate a large amount of oily wastewater, which may cause serious and long-term harm to the surrounding environment and ecological system [1–3]. Hence, research on effective treatment of oily wastewater has become a hotspot in the field of water purification. Traditional treatment of oily wastewater mainly involves centrifugation [4], bioremediation [5, 6], chemical catalytic decomposition [7, 8], air flotation [9], adsorption [10]. However, some of these methods have limitations like low efficiency, high cost and being time-consuming, which impede their practical application. Absorptive removal of oil using porous materials is a simple and effective technique. Therefore, much attention has been paid to the development of porous materials for potential application to clean up of oily pollutants.

Various porous materials have been utilized for absorptive separation or removal of oil from water, such as metal foam [11], polymer and carbon sponges [12, 13], fiber [14], zeolite [15] and aerogel [16]. Aerogel is a promising porous absorbent due to its three-dimensional (3D) porous structure, extremely low density, high porosity and large pore volume. These characteristics can lead to a high absorption capacity and quick absorption/desorption rates during the absorption process. Hydrophobic or superhydrophobic aerogels have been prepared as oil absorbent materials, such as graphene aerogel [17], nanofiber aerogel [18], cellulose aerogel [19], polymer aerogel [20] and silica aerogel. Carbon aerogel fabricated with carbon nanotubes and graphene possessed a low bulk density of 1.4 mg/cm^3 and exhibited excellent elasticity, the mass absorption capacity could reach 320 g/g for pump oil, which is higher than those of commercial materials.

Yi-Ming Li and Fang Liu have contributed equally to this work.

✉ Zai-Dong Shao
zdshao@iue.ac.cn

[1] Department of Materials Science and Engineering, College of Materials, Xiamen University, Xiamen 361005, Fujian, China

[2] CAS Key Laboratory of Urban Pollutant Conversion, Institute of Urban Environment, Chinese Academy of Sciences, Xiamen 361021, Fujian, China

[3] Fujian Key Laboratory of Advanced Materials, Xiamen 361005, Fujian, China

However, the use of aerogel as an absorbent in practical oil pollution treatment faces some challenges that need to be addressed. Firstly, commonly used oleophilic aerogel absorbents are complex to prepare, involving methods like supercritical drying or freeze-drying, which limits their practical and commercial application. Secondly, most prepared aerogel monoliths are used as static oil absorbents, but effective oil pollution treatment requires absorbents capable of separating oil from water [17]. Silica aerogel is a novel nanoporous material with low density and high porosity; it has attracted much attention due to its superhydrophobic property and could be fabricated through cost-effective ambient pressure drying (APD) [21]. However, the low integrity and poor mechanical properties of the silica aerogel prepared through APD have greatly limited its practical applications. Hence, the reinforcement of silica aerogel is important and has gained much attention in recent years.

The flexibility and elasticity of silica aerogels could be reinforced through polymer crosslinking [22], utilizing new silica precursors [23] and adding fibers [24]. However, reinforced silica aerogels have some drawbacks compared with pure silica aerogels, such as lower porosity and higher bulk density. Various studies have developed different reinforced silica aerogel monoliths using new silica precursors, such as methyltrimethoxysilane (MTMS)-based aerogel [25], co-precursor-based aerogel [26] and bridged robust silica aerogel [27, 28]. MTMS-based aerogel can absorb organic liquids and oils over 10 times its own mass [25]. Co-precursor-based silica aerogel with mesoporous structure exhibits good flexibility, elasticity and superhydrophobicity and can absorb trichloromethane by nearly eight times its dry weight [26]. However, the application of these aerogels is generally limited by tedious and complicated preparation and/or drying. Furthermore, most studies focused on the use of aerogels for batch absorption of oils from water, but few reports are available on the application of aerogels for oil/water separation.

Fiber reinforcement is another method used to obtain robust silica aerogel monolith. One conventional approach is dispersing micrometre-sized fibers in the silica aerogel matrix, and followed by supercritical drying (SCD) [29, 30]. However, the high brittleness and low compression strain (< 30%) can lead to cracking or fracturing. Harmful silica aerogel dusts could be released during force applications. Compared with micrometre-sized fibers, nanofibers possess a higher surface to volume ratio, which helps to increase the interaction between the nanofibers and composite matrix. The nanofibers can be homogeneously incorporated into the composite nanoporous silica aerogel matrix. Thus, nanofibers could be a promising material for the reinforcement of silica aerogels.

Nanofibers, including cellulose fiber, polypropylene fiber, polyaniline fiber, silica fiber and carbon fiber, have been studied and used to reinforce the silica aerogel matrix. Nanofibers can be fabricated using various methods, such as precipitation, hydrothermal, template synthesis, sol–gel and electrospinning. Cellulose nanofibers treated by aqueous alkali–urea solution have been used to reinforce silica aerogels, and the composite aerogels fabricated by SCD exhibited excellent flexibility, elasticity and deformation restorability. The result showed that the crosslinked cellulose nanofiber network could improve the brittleness of the SCD silica aerogel, which has a stretch modulus and a strength of 48.2 and 10.8 MPa, respectively, with a silica content of 39 wt%. However, the main drawbacks of this aerogel are low silica content (< 60 wt%), high density and high thermal conductivity [31].

Electrospinning is an effective and simple method used to prepare nanofibers with various polymers, such as polyvinylalcohol (PVA) [32], polyacrylonitrile (PAN) [33] and polyvinylidene fluoride (PVDF) [34]. A polyurethane (PU) nanofiber reinforced silica aerogel was fabricated by SCD after immersing the electrospun PU nanofiber film into silica sol. This aerogel could be bended without fracture and had a bending modulus and a yield strain of 5–10 and 150–200 MPa, respectively [35]. Flexible electrospun silica nanofiber-reinforced silica aerogel membranes were prepared by a similar process and applied as thermal insulating materials with tensile stress of 2–6.5 MPa [36]. However, electrospun nanofibers are usually collected on metal plate or rolling cylinder. The stacking of nanofibers in layers leads to a relatively dense non-woven film-like structures. As a result, electrospun nanofiber-reinforced silica aerogels are normally formed as films or sheets, which restricts the oil/water separation efficiency due to the limited amount of loaded silica aerogels and low porosity.

In our previous work, we reported a facile approach to fabricate high porosity (> 99%) 3D nanofibrous aerogel monolith principally through supporting agent liquid assisted collection-electrospinning technology and freeze-drying process. The nanofibrous aerogel had a combination of ultra-low density (2–3 $mg \cdot cm^{-3}$), high mechanical properties and good hydrophobicity. The unique porous characteristics of nanofibrous aerogel made it an excellent reinforcement for silica aerogel. To the best of our knowledge, the use of silica aerogel monoliths prepared and reinforced using electrospun nanofiber through APD for oil/water separation has not been reported yet. This makes our work an innovative effort [37].

In this work, we present a novel and simple strategy for the preparation of flexible electrospun PAN nanofiber-reinforced (EPNR) silica aerogel monolith through APD. The PAN nanofiber network was introduced into the hydrolysed silica sol by in situ electrospinning and liquid-assisted collection. Then the APD-EPNR silica aerogel was obtained after a two-step modification. The APD-EPNR silica aerogel

showed excellent flexibility, elasticity and surface hydrophobicity, which can be used for effective oil absorption and oil/water separation. The APD-EPNR silica aerogel appear to be a promising porous material for oil/water separation.

2 Experimental

2.1 Materials and chemicals

Tetraethoxysilane (TEOS) (≥ 98.0%), trimethylchlorosilane (TMCS) (≥ 98.0%), ethanol (≥ 99.7%), dimethylformamide (DMF) (≥ 98.0%), ammonia (25.0–28.0%), and n-hexane (≥ 97.0%) were purchased from Sinpharm Chemical Reagent Company, China, while methyltriethoxysilane (MTES) (≥ 98.0%) was from Shanghai Silicon Mountain Chemical Macromolecular Materials Company, China. The polyacrylonitrile (PAN) was obtained from Kunshan Hongyu Plastics Co., LTD., China.

2.2 Preparations of reinforced aerogels

The precursor solution for electrospinning was prepared by mixing PAN and DMF with the weight ratio of PAN:DMF = 1:9. The mixed solution was placed in a 10 mL plastic syringe equipped with a 21-gauge stainless steel needle. The prepared silica sol was poured into the collector container. The distance and voltage between the needle tips and the collector were set at 15 cm and 10 kV, respectively. The silica sol, which is composed of the molar ratios of TEOS: MTES: EtOH: H_2O as 1: 0.2: 10: 6, was continuously agitated for 12 h. After electrospinning was completed, ammonia was added to the silica sol to form wetgel. The composite silica wetgel was immersed into ethanol at 55 °C for 12 h to allow the strengthening of the gel network. The surface modification of the composite silica wetgel was carried out by immersion in the TMCS/ethanol/n-hexane solution at 35 °C for 48 h. The volume ratio of TMCS/ethanol/hexane was 2: 1: 8. Finally, the surface modified wetgel was washed by n-hexane to remove the remaining TMCS and then dried at atmospheric pressure in an oven at 80 °C. For comparison, supercritical dried PAN nanofiber-reinforced silica aerogel was prepared using a similar method but without adding MTES into the silica sol.

2.3 Organic solvents absorption capacity and water/oil separation of reinforced silica aerogel

The amounts of the APD-EPNR silica aerogel were weighed before and after oil absorption tests with various organic solvents. The mass-based oil absorption capacity (A_M) of the APD-EPNR silica aerogel was calculated by

$$A_M = \frac{M_F - M_1}{M_1} = \frac{\Delta M}{M_1} \tag{1}$$

where M_F and M_I are the weights of the APD-EPNR silica aerogel after and before the absorption, respectively. The volume-based oil absorption capacity (A_V) of the APD-EPNR silica aerogel was defined as

$$A_V = A_M \frac{\rho_a}{\rho_s} \tag{2}$$

where ρ_a and ρ_s are the bulk densities of the APD-EPNR silica aerogel and organic solvent, respectively.

Eleven organic solvents including benzene, toluene, liquid paraffin, chloroform, n-hexane, cyclohexane, phenol, simethicone, ethanol, n-heptane and tetrachloromethane were used.

The prepared APD-EPNR silica aerogel was used to separate oil/water mixture. Oil/water separation efficiency (K_s) was calculated by the formula

$$K_s = \frac{M_1}{M} \times 100\% \tag{3}$$

where M_I and M are the oil weights of the original oil/water mixture and the collected water after one cycle of separation, respectively. The volume ratio of the oil/water mixture was 1:1. Separation efficiency was measured three times, and the average value was used. In the recycled separation tests, after separation, the APD-EPNR silica aerogel used was washed with ethanol and dried at 80 °C.

2.4 Characterization of reinforced aerogels

Specific surface area, pore volume and pore size were estimated by nitrogen adsorption–desorption isotherm at 77 K (ASAP 2020, Micromeritics). Microscopic surface and cross-sectional morphologies were examined by scanning electron microscope (S-4800, Hitachi, Japan). Water contact angle was measured by contact angle meter (DSA100, Kruss, Germany). Chemical species and microstructure were investigated by Fourier transform infrared spectroscopy (Nicolet IS10, ThermoFisher Scientific). The thermal stability of the aerogel was studied by thermogravimetry (TG209F3, Netzsch, Germany). Compressive strain–stress test was performed on the aerogel specimen with a dimension of 10 mm × 10 mm × 15 mm by using a universal testing machine (KD-II 100N, KaiQiangLi, China).

3 Results and discussion

The preparation of in situ electrospun PAN nanofiber-reinforced silica aerogels is schematically illustrated in Fig. 1. The PAN nanofiber was electrospun into the hydrolysed

silica sol, according to liquid–solid interface theory. During electrospinning, the silica sol moved into the interspace of the nanofibrous network; thus, the PAN nanofibers were immersed homogeneously and formed a 3D network in the silica sol. After electrospinning, the silica precursor reacted with the basic catalyst added to obtain a composite gel. The composite wetgel was formed upon condensation and then immersed in ethanol to strengthen the silica network. The 3D PAN nanofiber network was incorporated by the silica aerogel. The aged composite silica wetgel was directly dried by SCD through Route I or modified by TMCS and followed by APD through Route II.

The photographs of the composite silica aerogels prepared through different drying routes are shown in Fig. 1 for comparison. Both aerogels showed excellent integrated monoliths without apparent cracks. The water contact angle of the APD-EPNR silica aerogel was 145°, indicating a highly hydrophobic surface; the surface of the SCD-EPNR silica aerogel was hydrophilic as expected. The incorporation of Si–C due to the MTES modification of the silica network and the TMCS modification of silica surface contributed to the hydrophobic property of the APD-EPNR silica aerogel.

The FT-IR spectra of PAN nanofiber and reinforced silica aerogels by different drying methods are shown in Fig. S1. The IR peaks in curves (a) at 2244 cm^{-1} and 1453 cm^{-1}, correspond to C≡N bending vibrations and -CH_2 flexural vibration, at 1621 cm^{-1} correspond to C = N and C = C, for PAN nanofiber [38]. Typical IR peaks in curves (b) and (c) correspond to Si–O-Si asymmetric, symmetric and rocking bending vibrations at 1080, 800 and 450 cm^{-1}, respectively, for silica materials. The peak at 1276 cm^{-1} and the shoulder at 847 cm^{-1} in curve (c) are related to Si–C bonding due to MTES modification of the silica network. Three additional peaks (1258, 867 and 758 cm^{-1}) were contributed by Si–C bonding, indicating that the silica network was further modified by TMCS. The co-precursor MTES modifies the silica cluster of the aerogel network as shown in Reaction (4). In the followed step, the modifying reagent TMCS reacts with the Si–OH group of the silica network to form Si-$(CH_3)_3$ through Reaction (5) [39].

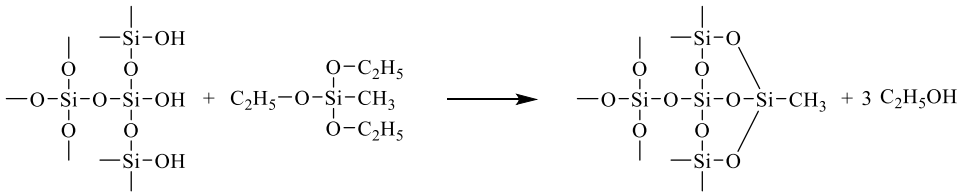

(4)

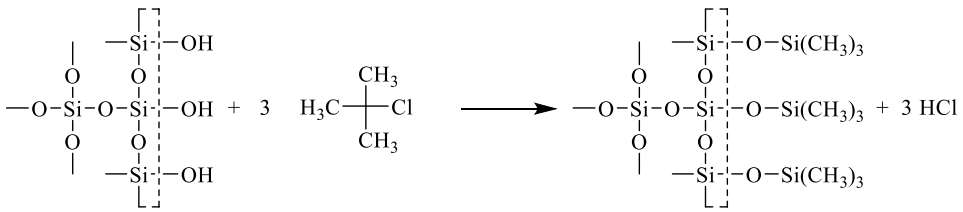

(5)

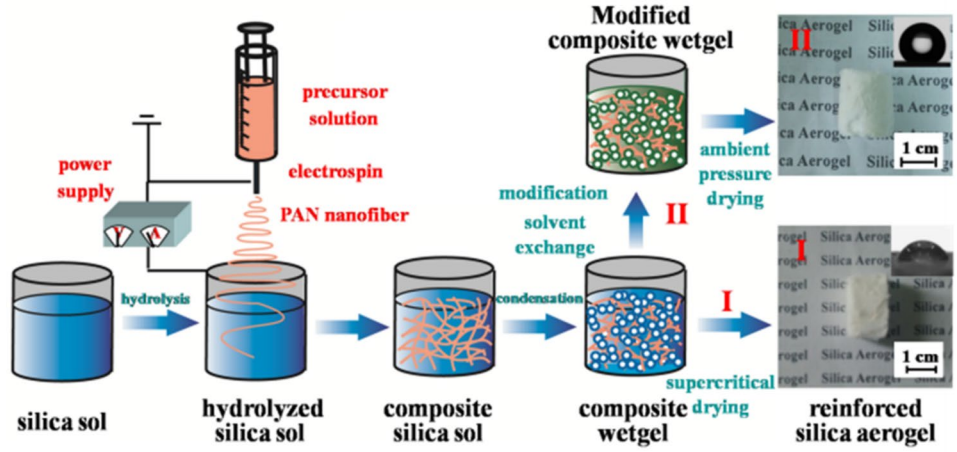

Fig. 1 Schematic representation for preparations of in situ electrospan PAN nanofiber reinforced silica aerogels via supercritical drying (Route I) and ambient pressure drying (Route II)

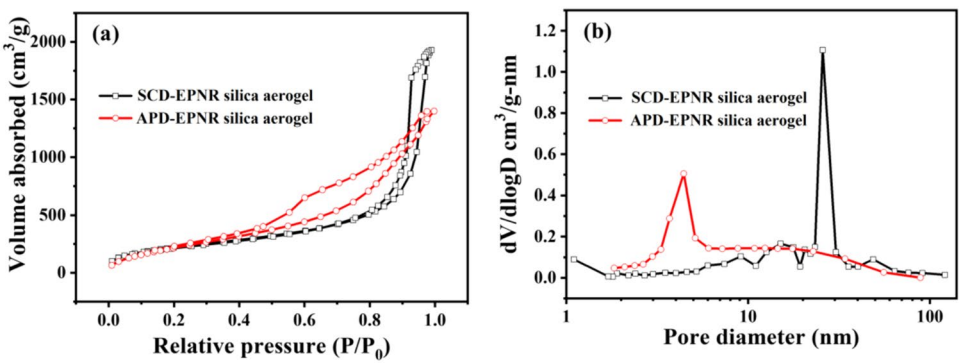

Fig. 2 Nitrogen adsorption–desorption isotherms (**a**) and pore size distribution curves (**b**) of EPNR silica aerogels by SCD and APD

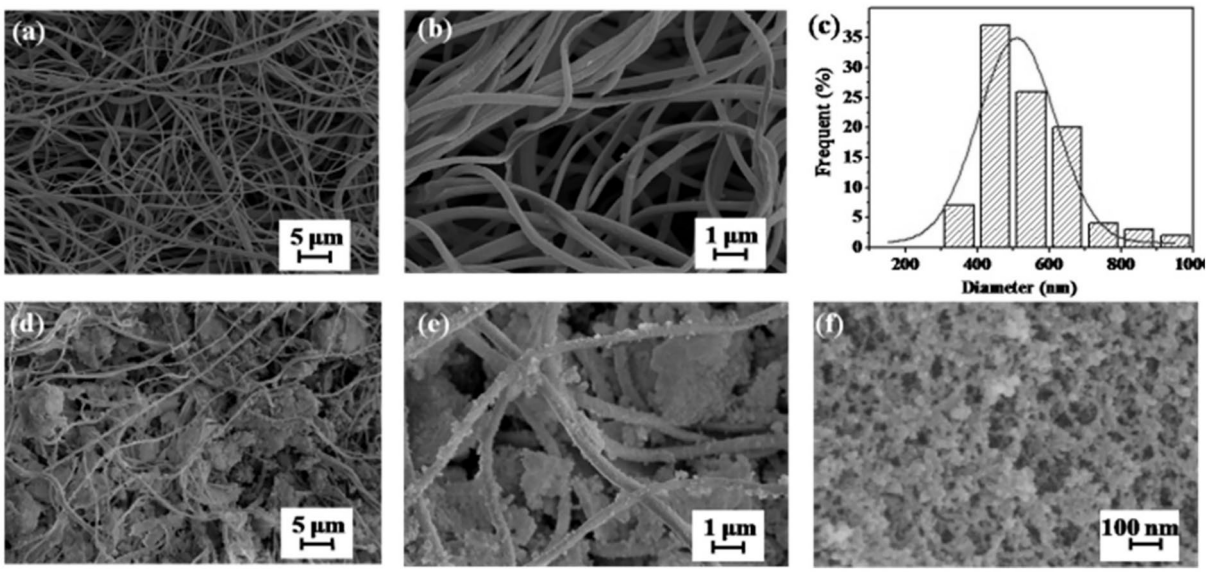

Fig. 3 SEM images (**a**–**b**), diameter distribution (**c**) of PAN nanofibers, APD-EPNR silica aerogel (**d**–**e**) and silica aerogel matrix by APD (**f**)

The nitrogen adsorption–desorption isotherms and pore distribution curves of the SCD-EPNR and APD-EPNR silica aerogel are compared in Fig. 2. The isotherm curves in Fig. 2a reveal a typical IV with a type H3 hysteresis loop, indicating a characteristic distribution of slit-shaped pores. The corresponding pore distribution curves in Fig. 2b differed from each other. The APD-EPNR silica aerogel had a pore distribution mainly in the range of 4–5 nm, with an average pore size of 6.3 nm. The pore distribution of SCD-EPNR silica aerogel is mainly in the range of 25–30 nm, and the average pore size was 10.5 nm. However, the BJH pore volume of the APD-EPNR silica aerogel was 2.15 $cm^3\ g^{-1}$, which is lower than that of the SCD-EPNR (3.00 $cm^3\ g^{-1}$), resulting in a slightly higher bulk density of 0.20 g cm^{-3} compared with the SCD-EPNR silica aerogel (0.11 g cm^{-3}). The BET specific surface area and porosity of the APD-EPNR silica aerogel silica aerogel were 890 $m^2\ g^{-1}$ and 90.9%, respectively, which are competitive to those of the SCD sample (807 $m^2\ g^{-1}$ and 95.0%, respectively). The nitrogen adsorption–desorption isotherms implied that the excellent physical properties of the APD-EPNR silica aerogel are protected by hydrophobic surface modification and APD. For SCD-EPNR silica aerogel, due to the lack of gas–solid interface during the supercritical drying process, the effect of capillary force on the skeletal aerogel network was avoided. Therefore, the higher pore volume (3.00 $cm^3\ g^{-1}$) and pore size (10.5 nm), and the lower bulk density (0.11 g cm^{-3}) were maintained. By contrast, the hydrophobic modification of APD-EPNR silica aerogel by MTES and TMCS can reduce the surface tension of the liquid in the pores during ambient pressure drying. The APD-EPNR silica aerogel with good surface modification would exhibit minor volume shrinkage during drying, so the APD-EPNR silica aerogel showed good physical properties with bulk density (0.20 g cm^{-3}), BJH pore volume (2.15 $cm^3\ g^{-1}$) and pore size (6.3 nm).

The surface morphologies of the PAN nanofibers and the APD-EPNR silica aerogel are shown in Fig. 3. The in situ electrospinning PAN nanofibers were randomly distributed with a 3D self-assembled loosened network structure and intertwined each other to form a continuous network (Fig. 3 and Fig S3a–b). The diameter distribution of PAN nanofibers conformed to the Gaussian distribution, mainly ranging from 300 to 500 nm (Fig. 3c), which benefits the uniform pore structure of the nanoporous silica aerogel. In addition, the presence of PAN nanofibers prevented the brittleness and fragment, making it an ideal matrix for silica aerogel

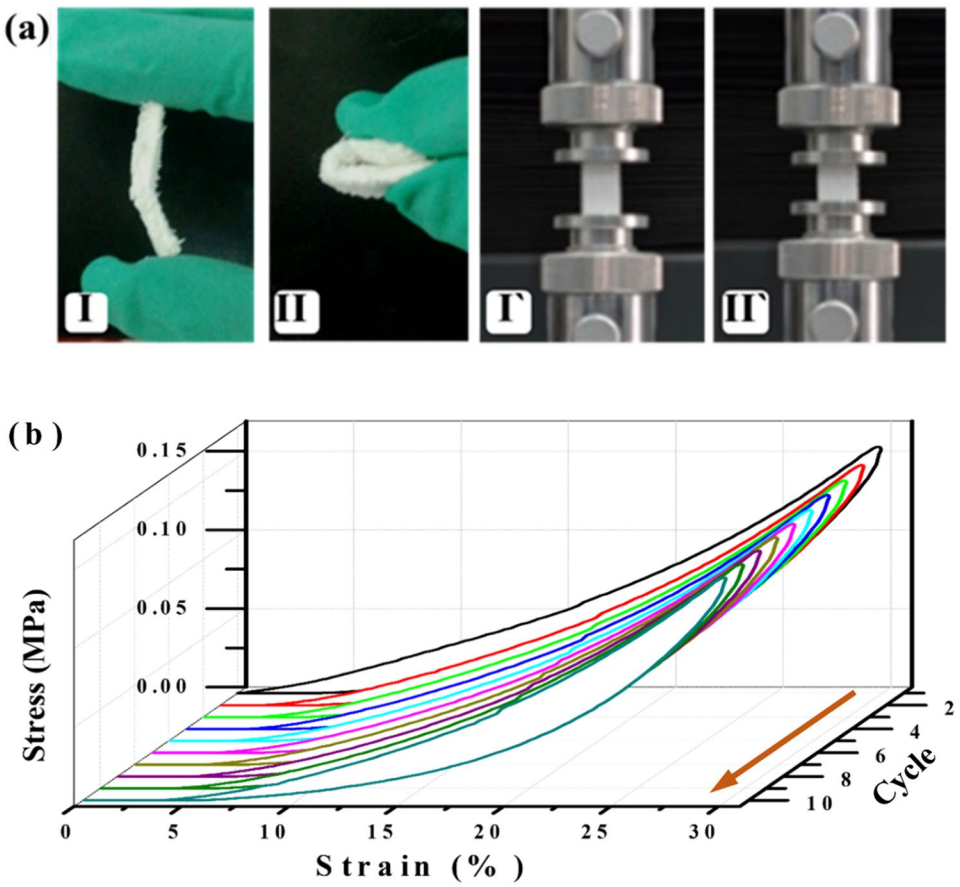

Fig. 4 Photographs showing good flexibility and elasticity (**a**), 10 cycles stress–strain curves of the of the APD-EPNR silica aerogels (**b**)

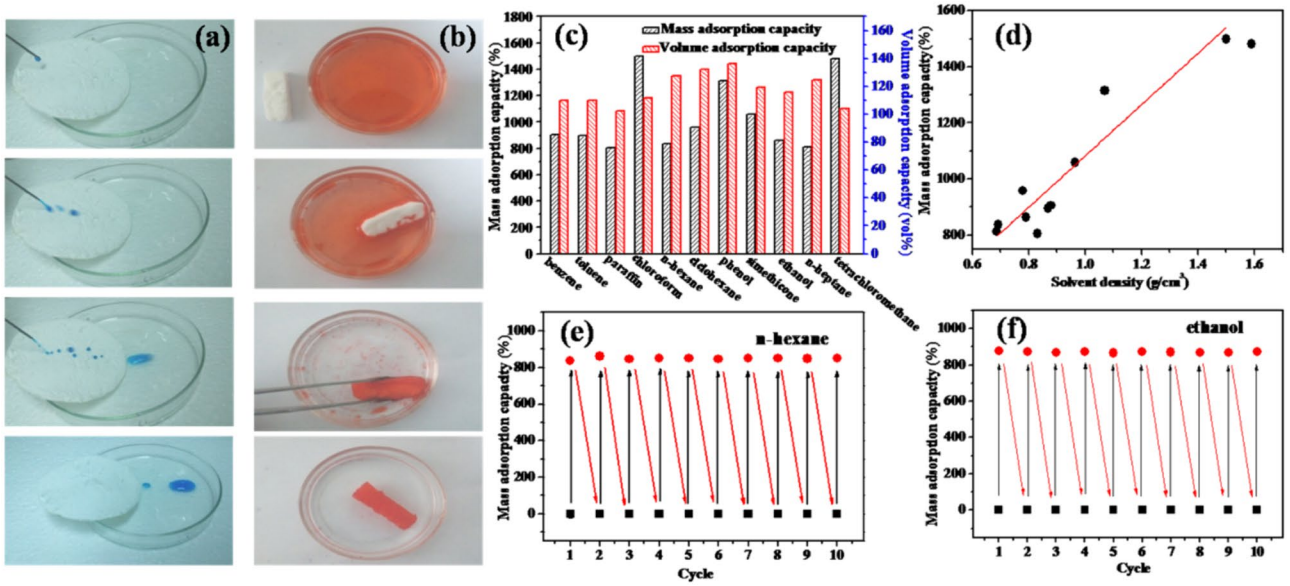

Fig. 5 Demonstration of the hydrophobicity and oleophilicity of the APD-EPNR silica aerogel: water droplets repelled away from the aerogel surface (**a**) and oil migrated from water surface to the aerogel (**b**), mass and volume absorption capacities of APD-EPNR silica aerogel for various organic solvents (**c**), mass absorption capacities for a range of organic solvents in terms of their densities (**d**), the cyclic absorption–desorption tests using n-hexane (**e**) and ethanol (**f**) as examples

(Fig. 3d, e). These fibers significantly reinforced the silica network structure compared with the unreinforced silica aerogel. Figure 3f and Fig. S3c showed the homodispersed and loosened network structure composed of nano-sized particles in the pure silica aerogel (without reinforcement). The comparison of SEM images revealed that there was no significant difference in the microscopic morphology between SCD-EPNR silica aerogel and APD-EPNR silica aerogel. The result proved that the APD-EPNR silica aerogel successfully overcomes the effect of capillary force and the nanopore structure was preserved. When force is applied, the interconnections between silica nanoparticles break continuously, resulting in obvious cracks until the pure silica aerogel fractures. However, in the PAN nanofiber-reinforced silica aerogel, the cracks were confined to the nanofiber gaps, and the silica aerogel fragments were held together by the PAN nanofibers. Even if the silica aerogel nanoskeleton cracked under pressure, the nanofibers enable it to withstand the external force while providing macroscopic flexibility. The TG curves in Fig. S3 showed a total weight loss of about 38.5% up to 800 °C for the APD-EPNR silica aerogel. This weight loss was due to the oxidation of PAN nanofiber and the modified methyl groups between 300 and 800 °C.

Figure 4a and Movies S1 and S2 demonstrate the excellent flexibility and elasticity of the APD-EPNR silica aerogel. The APD-EPNR silica aerogel retained its integrity and recovered without cracking or flaking even bending to 180°. The aerogel showed high compressibility, which can withstand multiple compressions and recover without apparent cracks. Figure 4b shows the accumulated stress–strain curves with the maximal strain of 30% for 10 continuous cycles. The APD-EPNR silica aerogel did not fully recover to its original shape and was slightly compressed after 10 cycles compression. The energy consumed (E_L) was evaluated by calculating the hysteresis loop area. The shrinkage in the stress–strain curves after 10 cycles indicates the accumulated energy losses. However, the APD-EPNR silica aerogel kept its monolithic shape without obvious cracks after each compression. The accumulated energy loss decreased rapidly from 754 to 585 kJ m^{-3} in the first two cycles and then decreased gradually with an increase in the cycle number (Fig. S4). The total energy loss was reduced to 462 kJ m^{-3} after 10 cycles (corresponding to a decrease of 38.7%).

The surface of the aerogel network was modified by MTES-TMCS, leading to a low surface energy. The resultant APD-EPNR silica aerogel exhibited hydrophobicity owing to the combination of the rough microstructure and the low surface energy. It showed high hydrophobicity and ultrafast absorption rate for organic solvents. As shown in Fig. 5a, the water droplets (coloured by methylene blue) slide off the APD-EPNR silica aerogel surface, while the liquid paraffin (coloured by Sudan red III) was absorbed completely by the aerogel monolith (Fig. 5b) due to the abundant mesopores and macropores in the aerogel network. The phenomenon indicates that the APD-EPNR silica aerogel could be used as oil absorption materials.

The capillary pressure (P) is the key driving force to absorb oil into hydrophobic aerogel. Assuming that the pores

shape of aerogel is cylindrical, the capillary pressure at oil-air interfaces in APD-EPNR silica aerogel can be expressed as:

$$P = \frac{2\gamma cos\theta}{r_m} \quad (6)$$

where γ is the surface tension at oil-air interfaces in aerogel pore, θ is the contact angle at oil-air interfaces, and r_m is the pore size of aerogel.

The capillary pressure is inversely proportional to the pore size of aerogel, the APD-EPNR silica aerogel exhibited excellent nanoporous property of high BET specific surface area (890 m^2 g^{-1}) and average pore size (10.5 nm). Therefore, it showed ultrafast absorption rate for organic solvents. The static mass and volume absorption capacities of the APD-EPNR silica aerogel for various solvents are shown in Fig. 5c. The APD-EPNR silica aerogel showed low bulk density (0.20 g cm^{-3}) and high porosity (90.9%), which indicated that the aerogel can provide abundant pores to storage oil. The mass absorption capacities of the APD-EPNR silica aerogel reached 700%-1500%, while a clear linearity was drawn between the mass absorption capacity and the density of the organic solvents (Fig. 5d). Hence, volume absorption capacity was used to evaluate the oil absorption performance (Fig. 5c). The volume absorption capacities of the APD-EPNR silica aerogel reached 100%-130% depending on the solvent, as the volume of the aerogel expanded during oil absorption. APD-EPNR silica aerogel also showed excellent cyclic absorption–desorption performance when n-hexane (Fig. 5e) and ethanol (Fig. 5f) were used for test. The aerogel absorbed > 800% n-hexane (by mass) in the first cycle, and the absorbed n-hexane was completely desorbed at 80 °C (Fig. 5e). During the 10 absorption–desorption cycles, the aerogel showed stable performance. Similar results were obtained for ethanol (Fig. 5f). Although ethanol has a greater potential to destroy the pore structure of the aerogel due to its higher surface tension coefficient compared with n-hexane. The aerogel network still showed stable performance, and no obvious absorption capacity was lost during the absorption–desorption test cycles. The cyclic performance results indicated that the absorbed oil APD-EPNR silica aerogel recovered oil by solvent exchange followed by evaporation. In summary, while the mass absorption capacities may not match some carbon aerogels, the APD-EPNR silica aerogel remains competitive due to the good volume absorption capacities, stable cyclic performance and cost-effective preparation. The oil absorption study suggested that the hydrophobic APD-EPNR silica aerogel is a good candidate for oil clean-up. For comparison, the physical properties and oil absorption performance of APD-EPNR silica aerogel and other reported silica aerogel were summarized in Table S1. The APD-EPNR silica aerogel possessed excellent physical properties, high mechanical performance and high oil absorption capacity.

For practical application in oil pollution treatment, oil absorbents should not only exhibit good static absorption performance, but also good oil/water separation

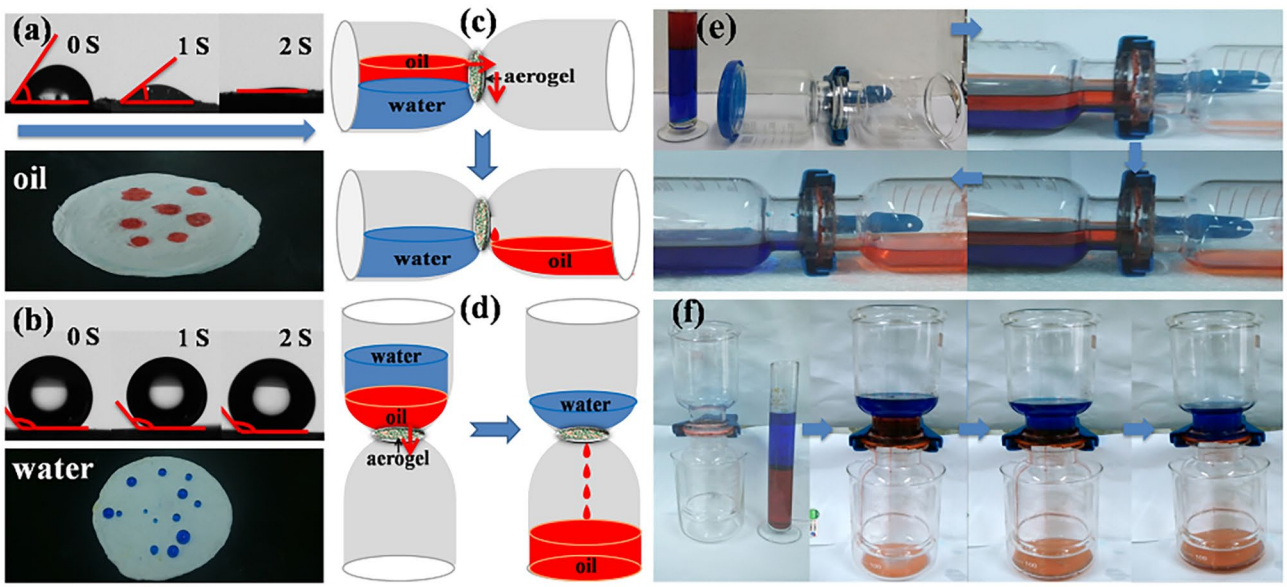

Fig. 6 The Dynamic water contact angle and photographs of oil wettability (**a**) and hydrophobicity (**b**) of the APD-EPNR silica aerogel mat, the schematic illustration (**c**, **d**) and separation processes (**e**, **f**) of selective oil/water separation devices. Aqueous phase was colored by methylene blue and the oil phase (paraffin oil) was colored by Sudan red III

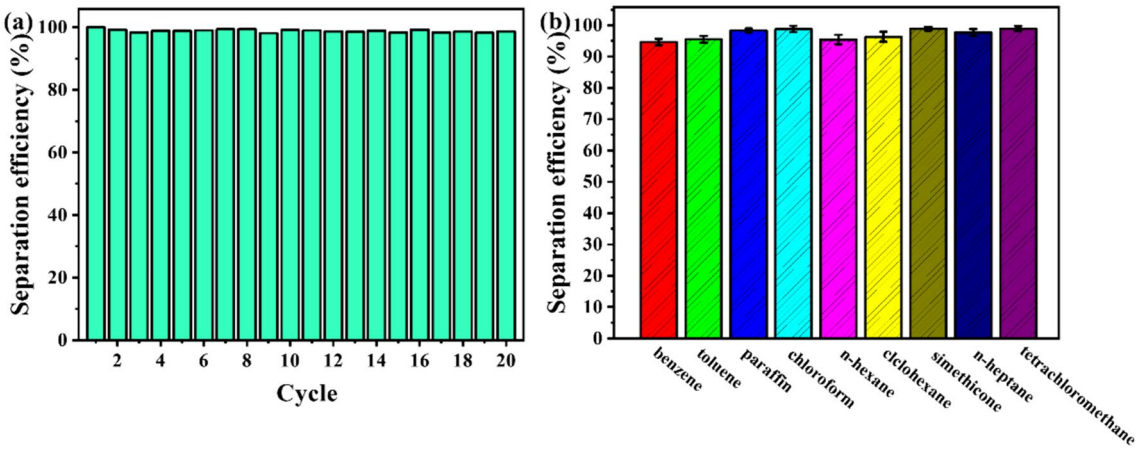

Fig. 7 The separation efficiency of prepared APD-EPNR silica aerogel for recyclability (**a**) and various organic solvents (**b**)

performance. The oil wettability of the APD-EPNR silica aerogel surface was investigated using the apparent contact angle. As shown in Fig. 6a, the paraffin oil was absorbed into the pore of the aerogel once the paraffin oil contacted to the surface, and the apparent contact angle quickly became zero. On the other hand, the APD-EPNR silica aerogel showed excellent hydrophobicity, and the water contact angle was 145° (Fig. 6b). The surface properties of the aerogel were confirmed by visual observation. The blue droplets (water) stayed on the aerogel surface, while paraffin oil droplets were immediately absorbed into the aerogel pores (Fig. 6a, b).

The APD-EPNR silica aerogel could be employed in oil/water separation due to its hydrophobicity and excellent mechanical properties. Figure 6c, d show the schematic of the oil/water separation device. Figure 6e, f show the visual photographs of the separation processes. The round aerogel monolith was placed in between two glass vessels. Similar to previous experiments, the oil phase was coloured by Sudan red III and the aqueous phase was coloured by methylene blue. Tetrachloromethane, which represent organic solvents that are denser than water, was selected to investigate the oil/water separation efficiency (Fig. 6d, f). The oil/water mixture was poured into the top flask, resulting in two immiscible phases (water on top and tetrachloromethane at the bottom. Driven by gravity only, the tetrachloromethane quickly passed through the aerogel and settling in the bottom flask, while the water was blocked by the hydrophobic APD-EPNR silica aerogel. A different setup was deployed to evaluate the separation efficiency of the aerogel when the density of the organic solvents was lower than water (Fig. 6c). The n-hexane/water mixture was used as a representative in this case (Fig. 6e). The red n-hexane penetrated the APD-EPNR silica aerogel and dropped to the second vessel without external force, while water was retained in the original vessel. The APD-EPNR silica aerogel had higher oil/water separation efficiency than the original brittle aerogel.

Reusability is an important criterion used to evaluate oil/water separation performance. The separation efficiency of the prepared APD-EPNR silica aerogel was tested over 20 cycles of separation and the results are shown in Fig. 7a. The tetrachloromethane/water mixture was used to evaluate recyclability. In general, the separation efficiency reached 99% and no obvious decline was observed throughout the 20 cycles of separation. The high separation efficiency, excellent stability and reusability of the prepared APD-EPNR silica aerogel make it promising for oil/water separation. The versatility of the prepared APD-EPNR silica aerogel was assessed by evaluating the separation efficiencies for the mixture of water and nine different organic solvents. High separation efficiencies, ranging from 95 to 99%, were obtained (Fig. 7b), indicating that the APD-EPNR silica aerogel could be a viable option for the separation of various organic solvents and oils from water.

4 Conclusions

The continuous PAN nanofiber with a three-dimensional network was prepared by electrospinning and liquid-assisted collection. The PAN nanofiber was used to in situ strengthen the network of the silica aerogel. The electrospun PAN nanofiber-reinforced silica aerogel monolith, which was synthesised by drying at atmospheric pressure, was flexible and highly hydrophobic. The BET specific surface area of 890 m^2 g^{-1} and the BJH pore volume of

2.15 $cm^3 g^{-1}$ were achieved. The obtained aerogel could be used to remove oil from water. Furthermore, the oil/water separation device was designed and could be effectively used for the separation of oil/water mixture. The method in this study is suitable for large-scale fabrication and has potential applications in oil/water separation.

Supplementary Information The online version contains supplementary material available at https://doi.org/10.1007/s10934-024-01625-5.

Acknowledgements This work was financially supported by the National Natural Science Foundation of China (No. 52370122), the STS Project of Science and Technology Program of Fujian Province (No. 2023T3014), the Science and Technology Planning Project of Fujian Province (No. 2021H0050), the Youth Innovation Promotion Association CAS (No. 2019307), the Science and Technology planning Project of Xiamen City (No. 3502Z20191021), the Science and Technology Innovation "2025" major program in Ningbo (No. 2022Z028).

Author contributions Yi-Ming Li: Data curation, Writing—original draft. Fang Liu: Data curation, Writing—original draft. Zhen-Zhen Jia: Investigation. Xuan Cheng: Investigation. Yu-Ming Zheng: Investigation, Funding acquisition. Zai-Dong Shao: Writing—review & editing, Supervision, Funding acquisition.

Declarations

Competing interest The authors declare that they have no conflict of interest and no competing financial interest.

References

1. J.Y. Zhang, F. Zhang, W.X. Fang, J. Jin, Membrane wettability manipulation via mixed-dimensional heterostructured surface towards highly efficient oil-in-water emulsion separation. J. Membr. Sci. **672**, 121472 (2023). https://doi.org/10.1016/j.memsci.2023.121472
2. J.F. Wu, Z.W. Cui, Y.X. Su, Y. Yu, B. Yue, J.D. Hu, J.F. Qu, D. Tian, X.X. Zhan, J.Z. Li, Y.H. Cai, Biomimetic cellulose-nanocrystalline-based composite membrane with high flux for efficient purification of oil-in-water emulsions. J. Hazard. Mater. **446**, 130729 (2023). https://doi.org/10.1016/j.jhazmat.2023.130729
3. W.B. Che, L.Y. Zhou, Q.R. Zhou, Y.J. Xie, Y.G. Wang, Flexible Janus wood membrane with asymmetric wettability for high-efficient switchable oil/water emulsion separation. J. Colloid Interf. Sci. **629**, 719–727 (2023). https://doi.org/10.1016/j.jcis.2022.09.109
4. D. Allende, A. Cambiella, J.M. Benito, C. Pazos, J. Coca, Destabilization-enhanced centrifugation of metalworking oil-in-water emulsions: effect of demulsifying agents. Chem. Eng. Technol. **31**(7), 1007–1014 (2008). https://doi.org/10.1002/ceat.200700018
5. A. Karim, M.A. Islam, Z.B. Khalid, Y. Abu, M.M.R. Khan, C.K.M. Faizal, Microbial lipid accumulation through bioremediation of palm oil mill effluent using a yeast-bacteria co-culture. Renew. Energy **176**, 106–114 (2021). https://doi.org/10.1016/j.renene.2021.05.055
6. R.P.J. Swannell, K. Lee, M. McDonagh, Field evaluations of marine oil spill bioremediation. Microbiol. Rev. **60**(2), 342–365 (1996). https://doi.org/10.1128/mmbr.60.2.342-365.1996
7. Z.Z. Chen, X.R. Zhang, L. Che, H.H. Peng, S.X. Zhu, F. Yang, X. Zhang, Effect of volatile reactions on oil production and composition in thermal and catalytic pyrolysis of polyethylene. Fuel **271**, 117308 (2020). https://doi.org/10.1016/j.fuel.2020.117308
8. E.B. Kujawinski, M.C.K. Soule, D.L. Valentine, A.K. Boysen, K. Longnecker, M.C. Redmond, Fate of dispersants associated with the deepwater horizon oil spill. Environ. Sci. Technol. **45**(4), 1298–1306 (2011). https://doi.org/10.1021/es103838p
9. J. Lee, W.C. Cho, K.M. Poo, S. Choi, T.N. Kim, E.B. Son, Y.J. Choi, Y.M. Kim, K.J. Chae, Refractory oil wastewater treatment by dissolved air flotation, electrochemical advanced oxidation process, and magnetic biochar integrated system. J. Water Process. Eng. **36**, 101358 (2020). https://doi.org/10.1016/j.jwpe.2020.101358
10. M. Fouladi, M. Kavousi Heidari, O. Tavakoli, Development of porous biodegradable sorbents for oil/water separation: a critical review. J. Porous Mat. **30**, 1037–1053 (2022). https://doi.org/10.1007/s10934-022-01385-0
11. N. Chen, Q.M. Pan, Versatile fabrication of ultralight magnetic foams and application for oil-water separation. ACS Nano **7**(8), 6875–6883 (2013). https://doi.org/10.1021/nn4020533
12. X.C. Dong, J. Chen, Y.W. Ma, J. Wang, M.B. Chan-Park, X.M. Liu, L.H. Wang, Superhydrophobic and superoleophilic hybrid foam of graphene and carbon nanotube for selective removal of oils or organic solvents from the surface of water. Chem. Commun. **48**(86), 10660–10662 (2012). https://doi.org/10.1039/c2cc35844a
13. J.F. Lu, X. Liu, T.C. Zhang, H.Q. He, S.J. Yuan, Magnetic superhydrophobic polyurethane sponge modified with bioinspired stearic acid@Fe_3O_4@PDA nanocomposites for oil/ water separation. Colloid Surf. A-Physicochem. Eng. Asp. **624**, 126794 (2021). https://doi.org/10.1016/j.colsurfa.2021.126794
14. A. Bayat, S.F. Aghamiri, A. Moheb, G.R. Vakili-Nezhaad, Oil spill cleanup from sea water by sorbent materials. Chem. Eng. Technol. **28**(12), 1525–1528 (2005). https://doi.org/10.1002/ceat.200407083
15. J.K. Pan, Y.Y. Ge, Low-cost and high-stability superhydrophilic/underwater superoleophobic NaA zeolite/copper mesh composite membranes for oil/water separation. Surf. Interf. **37**, 102703 (2023). https://doi.org/10.1016/j.surfin.2023.102703
16. Y. Yi, P. Liu, N. Zhang, M.E. Gibril, F. Kong, S. Wang, A high lignin-content, ultralight, and hydrophobic aerogel for oil-water separation: preparation and characterization. J. Porous Mat. **28**, 1881–1894 (2021). https://doi.org/10.1007/s10934-021-01129-6
17. X.L. Ma, Z.S. Kong, Y. Gao, Y.N. Bai, W.Y. Wang, H.L. Tan, X.M. Cai, J.M. Cai, Anisotropic free-standing aerogels based on graphene/silk for pressure sensing and efficient adsorption. ACS Appl. Mater. Interf. **15**(25), 30630–30642 (2023). https://doi.org/10.1021/acsami.3c03659
18. X.H. Ge, Y.F. Zhang, X. Li, C. Chen, J. Jin, T.Q. Liang, J. Liu, W.W. Lei, D. Shi, Rational design of polymer nanofiber aerogels with aligned micrometer-sized porous structures and their high separation performance. ACS Appl. Compos. Commun. **38**, 101527 (2023). https://doi.org/10.1016/j.coco.2023.101527
19. L.T. Mo, H.W. Pang, Y.T. Lu, Z. Li, H.J. Kang, M.G. Wang, S.F. Zhang, J.Z. Li, Wood-inspired nanocellulose aerogel adsorbents with excellent selective pollutants capture, superfast adsorption, and easy regeneration. J. Hazard. Mater. **415**, 125612 (2021). https://doi.org/10.1016/j.jhazmat.2021.125612
20. O. Karatum, S.A. Steiner, J.S. Griffin, W.B. Shi, D.L. Plata, Flexible, mechanically durable aerogel composites for oil capture and recovery. ACS Appl. Mater. Interf. **8**(1), 215–224 (2016). https://doi.org/10.1021/acsami.5b08439
21. N. Husing, U. Schubert, Aerogels airy materials: chemistry, structure, and properties. Angew. Chem. Int. Edit. **37**(1–2), 23–45 (1998). https://doi.org/10.1021/acsami.5b08439

22. H.Q. Guo, M.A.B. Meador, L. McCorkle, D.J. Quade, J. Guo, B. Hamilton, M. Cakmak, Tailoring properties of cross-linked polyimide aerogels for better moisture resistance, flexibility, and strength. ACS Appl. Mater. Interf. **4**(10), 5422–5429 (2012). https://doi.org/10.1021/am301347a
23. S. Yun, H.J. Luo, Y.F. Gao, Low-density, hydrophobic, highly flexible ambientpressure- dried monolithic bridged silsesquioxane aerogels. J. Mater. Chem. A. **3**(7), 3390–3398 (2015). https://doi.org/10.1039/c4ta05271d
24. S.B. Jadhav, A. Makki, D. Hajjar, P.B. Sarawade, Synthesis of light weight recron fiber-reinforced sodium silicate based silica aerogel blankets at an ambient pressure for thermal protection. J. Porous Mat. **29**, 957–969 (2022). https://doi.org/10.1007/s10934-022-01231-3
25. D.J. Chen, K.Y. Dong, H.Y. Gao, T. Zhuang, X.B. Huang, G. Wang, Vacuum-dried flexible hydrophobic aerogels using bridged methylsiloxane as reinforcement: performance regulation with alkylorthosilicate or alkyltrimethoxysilane co-precursors. New J. Chem. **43**(5), 2204–2212 (2019). https://doi.org/10.1039/c8nj04038a
26. J.F. Ren, X. Huang, J.J. Shi, W. Wang, J.N. Li, Y. Zhang, H.K. Chen, R.L. Han, G.X. Chen, Q.F. Li, Z. Zhou, Transparent, robust, and machinable hybrid silica aerogel with a "rigid-flexible" combined structure for thermal insulation, oil/water separation, and self-cleaning. J. Colloid Interf. Sci. **623**, 1101–1110 (2022). https://doi.org/10.1016/j.jcis.2022.05.100
27. Z. Wang, Z. Dai, J.J. Wu, N. Zhao, J. Xu, Vacuum-dried robust bridged silsesquioxane aerogels. Adv. Mater. **25**(32), 4494–4497 (2013). https://doi.org/10.1002/adma.201301617
28. Z. Wang, D. Wang, Z.C. Qian, J. Guo, H.X. Dong, N. Zhao, J. Xu, Robust superhydrophobic bridged sils esquioxane aerogels with tunable performances and their applications. ACS Appl. Mater. Interf. **7**(3), 2016–2024 (2015). https://doi.org/10.1021/am5077765
29. Z.D. Shao, X.Y. He, Z.W. Niu, T. Huang, X. Cheng, Y. Zhang, Ambient pressure dried shape-controllable sodium silicate based composite silica aerogel monoliths. Mater. Chem. Phys. **162**, 346–353 (2015). https://doi.org/10.1016/j.matchemphys.2015.05.077
30. T. Linhares, M.T.P. de Amorim, L. Duraes, Silica aerogel composites with embedded fibres: a review on their preparation, properties and applications. J. Mater. Chem. A. **7**(40), 22768–22802 (2019). https://doi.org/10.1039/c9ta04811a
31. J. Cai, S.L. Liu, J. Feng, S. Kimura, M. Wada, S. Kuga, L.N. Zhang, Cellulose-Silica Nanocomposite Aerogels by In Situ Formation of Silica in Cellulose Gel. Angew. Chem. Int. Edit. **51**(9), 2076–2079 (2012). https://doi.org/10.1002/anie.201105730
32. H.L. Lin, S.H. Wang, Nafion/poly(vinyl alcohol) nano-fiber composite and Nafion/poly(vinyl alcohol) blend membranes for direct methanol fuel cells. J. Membr. Sci. **452**, 253–262 (2014). https://doi.org/10.1016/j.memsci.2013.09.039
33. C. Tran, V. Kalra, Co-continuous nanoscale assembly of Nafion-polyacrylonitrile blends within nanofibers: a facile route to fabrication of porous nanofibers. Soft Matter **9**(3), 846–852 (2013). https://doi.org/10.1039/c2sm25976a
34. C.L. Liu, X.F. Li, T. Liu, Z. Liu, N.N. Li, Y.F. Zhang, C.F. Xiao, X.S. Feng, Microporous CA/PVDF membranes based on electrospun nanofibers with controlled crosslinking induced by solvent vapor. J. Membr. Sci. **512**, 1–12 (2016). https://doi.org/10.1016/j.memsci.2016.03.062
35. L.C. Li, B. Yalcin, B.N. Nguyen, M.A.B. Meador, M. Cakmak, Flexible nanofiber-reinforced aerogel (xerogel) synthesis, manufacture, and characterization. ACS Appl. Mater. Interf. **1**(11), 2491–2501 (2009). https://doi.org/10.1021/am900451x
36. H.X. Zheng, H.R. Shan, Y. Bai, X.F. Wang, L.F. Liu, J.Y. Yu, B. Ding, Assembly of silica aerogels within silica nanofibers: towards a super-insulating flexible hybrid aerogel membrane. RSC Adv. **5**(111), 91813–91820 (2015). https://doi.org/10.1039/c5ra18137b
37. Y.Z. Lin, L.B. Zhong, S. Dou, Z.D. Shao, Q. Liu, Y.M. Zheng, Facile synthesis of electrospun carbon nanofiber/graphene oxide composite aerogels for high efficiency oils absorption. Environ. Int. **128**, 37–45 (2019). https://doi.org/10.1016/j.envint.2019.04.019
38. Y. Zhang, Y.L. Rena, X.H. Liu, T.G. Huo, Y.W. Qin, Preparation of durable flame retardant PAN fabrics based on amidoximation and phosphorylation. Appl. Surf. Sci. **428**, 395–403 (2018). https://doi.org/10.1016/j.apsusc.2017.09.155
39. S.A. Mahadik, M.S. Kavale, S.K. Mukherjee, A.V. Rao, Transparent Superhydrophobic silica coatings on glass by sol-gel method. Appl. Surf. Sci. **257**(2), 333–339 (2010). https://doi.org/10.1016/j.apsusc.2010.06.062